Materials Chemistry and Physics 287 (2022) 126358

Contents lists available at ScienceDirect

Materials Chemistry and Physics

journal homepage: www.elsevier.com/locate/matchemphys

Engineering hydrated vanadium oxide by K^+ and Ni^{2+} incorporation for aqueous zinc ion batteries

Sean Li, Xiaoxiao Jia, Junchao Liu, Ziyan Liu, Guozhong Cao *

Department of Materials Science and Engineering, University of Washington, Seattle, WA, 98195, USA

HIGHLIGHTS

- Highlights (for review).
- KNiVOH as ZIBs' cathode material demonstrated high capacity and good cycle performance.
- Incorporating of Ni^{2+} is believed to facilitate the electronic conductivity and the Zn^{2+} intercalation kinetics in KNiVOH.
- KNiVOH has the smallest polarization than VOH, KVOH and NiVOH due to its smallest voltage gap of the redox pair V^{5+}/V^{4+}.
- KNiVOH owns the highest capacitive contribution than VOH, KVOH and NiVOH owing to its fast transport property.

ABSTRACT

It is confirmed that K^+ introduction is a feasible approach to lead hydrated vanadium pentoxide to a new phase of KVOH which is considered a cathode material with substantial potential for aqueous zinc ion batteries (ZIBs). Nevertheless, the desire to pursue higher value of specific capacity is still a barrier to its development of applications. Herein, a Ni-doped KVOH (KNiVOH) is developed to achieve higher value of specific capacity. Besides, Ni^{2+} introduction can intensify the conductivity and encourage the electronic rearrangement, which is advantageous to the electrochemical characteristic and chemical kinetics of the KNiVOH. Furthermore, Ni^{2+} can make KVOH's K–O bond become more stable by decreasing the energy of formation. As regards the specific capacity value, KNiVOH displays the value of 275 mAh g^{-1} at 5A g^{-1}, which is better than KVOH (266 mAh g^{-1}). Consequently, these properties recommend KNiVOH as a promising cathode material candidate of ZIBs, indicating it is a practical strategy to combine potassium with other transition metals to synthesize new cathode materials for ZIBs in the future.

1. Introduction

The ever-growing worldwide energy demand and approaching anxiety about severe green issues have aroused the advancement of progressive storage battery systems. Lithium ion batteries (LIBs) have been broadly explored and have made great achievement in commercial purpose and discovered extensive uses during past several decades, nowadays being prevalent in most people's daily lives [1,2]. However, the continuing worries about security, great expense, scarcity of lithium, and environmental hazards have hindered the uses of LIBs and stimulated the scientists to explore other possible substitutes [3]. Besides, secure, innocuous, and cheap aqueous electrolytes are now all the rage as green chemistry become more and more prevalent [4]. First of all, avoidance of combustible organic electrolytes. In addition, aqueous electrolytes possess higher ionic conductivity which empowers faster charge/discharge rate [5]. What's more, the aqueous rechargeable batteries are cheaper and more convenient to be assembled than organic LIBs [6]. Recently, scientists put effort into aqueous rechargeable batteries as well as search for inexpensive metal ions: K^+ [7], Al^{3+} [8] and Zn^{2+} [9], for instance. Compare with other possible candidates, Zn^{2+} is the most attractive one due to intrinsic superiority of Zn metal as following (Table S1): affordable price owing to abundant production [10]; innocuous, convenient and full-grown process; high value of anode capacity in theory (820 mAh g^{-1}) owing to double-electron redox characteristic [5,10]; high value of volumetric energy density (5851 mAh cm^{-3}) [10]; and promising operational stability in aqueous electrolytes. Consequently, aqueous ZIBs are attractive storage battery systems which possess cathode made of materials with Zn ions intercalation, anode made of Zn metal, and electrolyte made of slightly acidic or neutral Zn-containing solutions.

As for the advancement of aqueous ZIBs, scientists put emphasis on two aspects: clearing up the chemical mechanisms of electrochemistry and utilizing suitable cathode materials. Several aqueous ZIBs cathode materials have been suggested in recent years: manganese oxides [11]

* Corresponding author.
E-mail address: gzcao@uw.edu (G. Cao).

https://doi.org/10.1016/j.matchemphys.2022.126358
Received 29 January 2022; Received in revised form 15 May 2022; Accepted 4 June 2022
Available online 5 June 2022

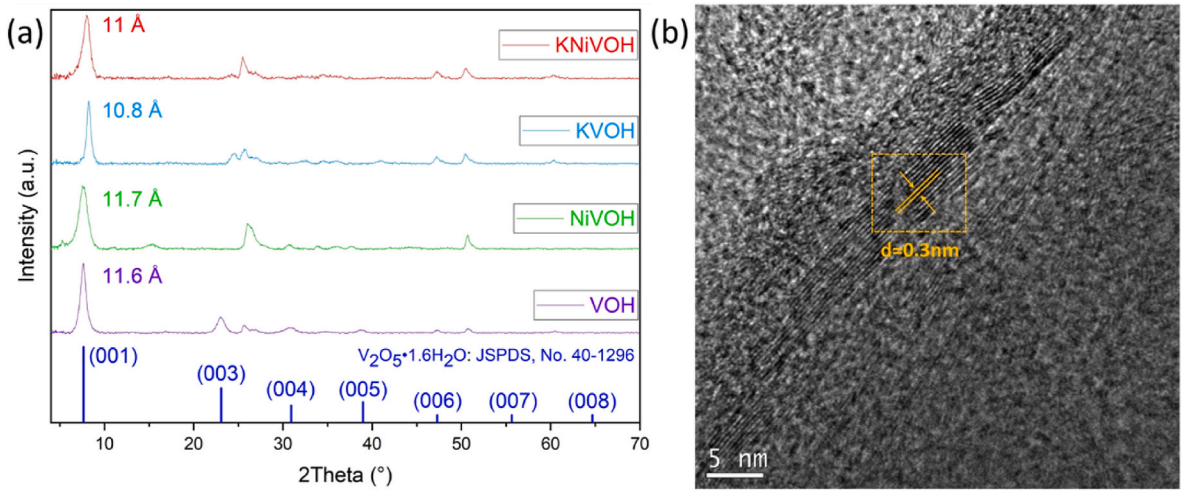

Fig. 1. (a) Comparison of XRD patterns of KNiVOH, KVOH, NiVOH and VOH. (b) HR-TEM image of KNiVOH.

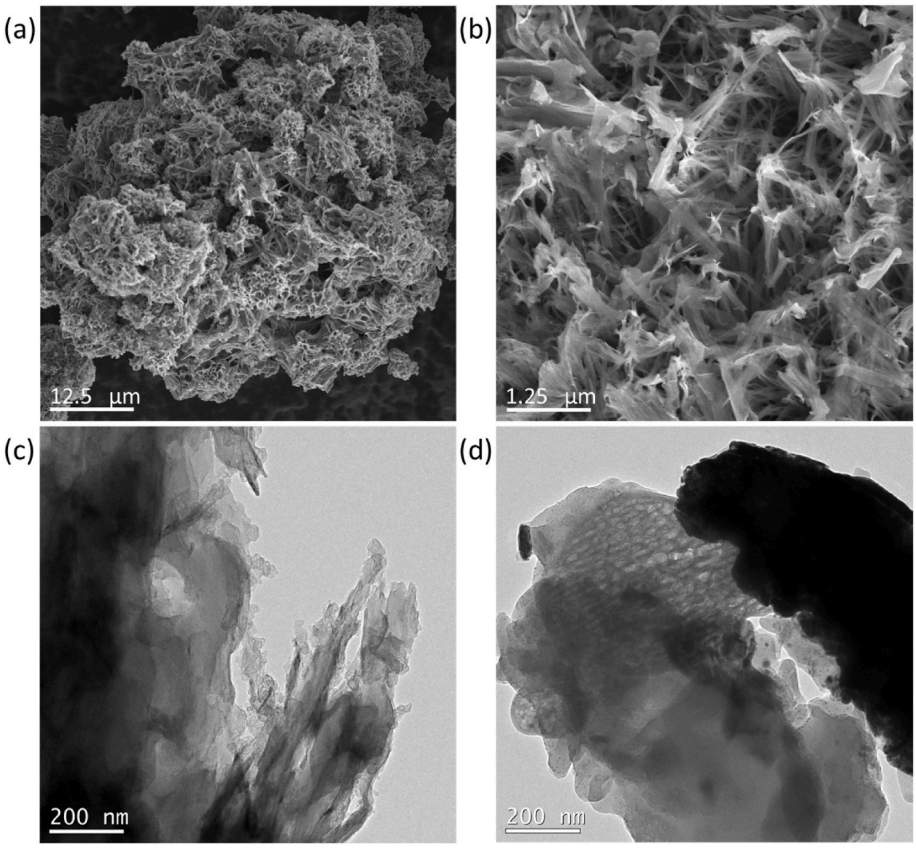

Fig. 2. Structural characterization of KNiVOH with SEM and TEM. (a) Low magnification SEM image revealing the range of microsphere's diameter is 75–80 μm. (b) High magnification SEM image illustrating that the microspheres are consisted of numerous nanorods. (c) TEM image confirming the aggregation of nanorods in Fig. 2a. (d) TEM image showing that KNiVOH has porous structure.

and vanadium oxides [12]. Owing to profusion, layered crystal structure which can enable plenty of Zn^{2+} intercalation [13], and high value of specific capacity, vanadium oxides has caught most scientists' eyes.

Nonetheless, structural instability during repeated intercalation/deintercalation of Zn^{2+} should be modified in order to achieve the needs for commercial purposes [14]. A crucial approach is to pre-intercalate foreign metal ions or structural water into the interlayers of material's structure in order to expand the interlayer spacing, which can be helpful for higher speed of ion diffusion and more stable electrochemical properties [15]. The molecules of structural water supply the function of charge shielding which can decrease the electrostatic interaction between Zn^{2+} and V_2O_5 skeleton [16], hence nourish the kinetics aspect of Zn^{2+} intercalation. Putting metal ions between layer-structured vanadium oxides is also an efficacious method [17]. A successful strategy is by putting transition metal ions like Mn^{2+} between layer-structured hydrated vanadate in order to expand the interlayer spacing. By doing so, hydrated vanadate would result in MnVO, which is a cathode material that possesses both structural and thermodynamic stability. MnVO

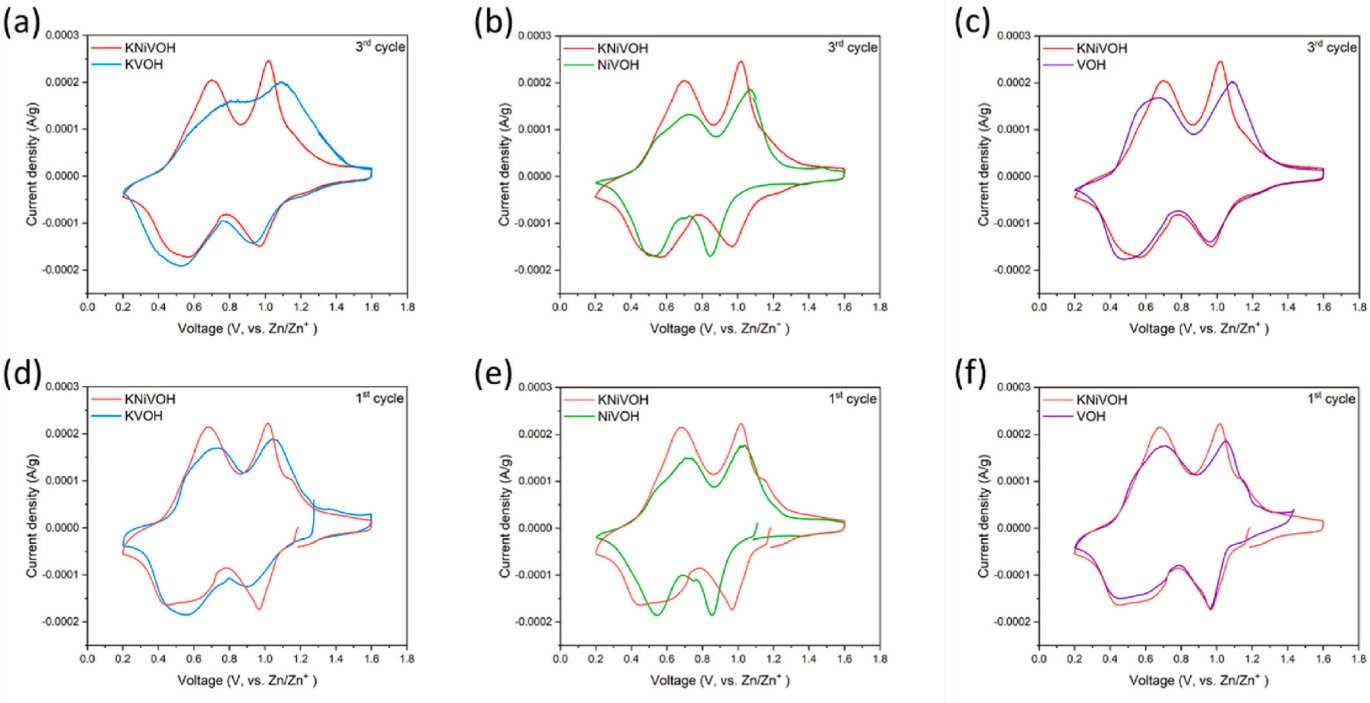

Fig. 3. (a) KNiVOH and KVOH, (b) KNiVOH and NiVOH, (c) KNiVOH and VOH show the 3rd cycle CV curves comparison at 0.1 mV s^{-1}. (d) KNiVOH and KVOH, (e) KNiVOH and NiVOH, (f) KNiVOH and VOH show the 1st cycle CV curves comparison at 0.1 mV s^{-1}.

Table 1
Comparison at 0.1 mV s^{-1} (3rd cycle CV curves) of the peaks positions, voltage gaps and center positions in KNiVOH, KVOH, NiVOH and VOH.

Sample		Peak position	Voltage gap	Center position
KNiVOH	V^{5+}/V^{4+}	1.02/0.96	0.06	0.99
KVOH	V^{5+}/V^{4+}	1.08/0.96	0.13	1.02
NiVOH	V^{5+}/V^{4+}	1.09/0.93	0.16	1.01
VOH	V^{5+}/V^{4+}	1.07/0.84	0.23	0.96
KNiVOH	V^{4+}/V^{3+}	0.71/0.56	0.14	0.63
KVOH	V^{4+}/V^{3+}	0.67/0.47	0.20	0.57
NiVOH	V^{4+}/V^{3+}	0.80/0.51	0.29	0.65
VOH	V^{4+}/V^{3+}	0.73/0.50	0.23	0.62

owns interplanar spacing value of 12.9 Å, and it also shows cycling stability with capacity retention value of 92% over 2000 cycles and high specific capacity value of 415 mAh g^{-1} at current density value of 0.05 A g^{-1}, which is notably finer than hydrated vanadium pentoxide (VOH).

It is reasonable assumed that due to the pillar effect which can strengthen the stability of layered crystal structure, so MnVO has better performance in cycling stability than VOH [18]. In addition, Zn^{2+}, Ni^{2+}, and La^{3+} also are good choices to be intercalated into hydrated vanadates to strengthen electrochemical performance [19]. What's more, scientists found out that alkaline metal ions, which are inexpensive, own just the same pillar effect as transition metal ions in order to make vanadate structure become more stable [20]. Among the alkaline metal ions, because K^+ ions own the largest atomic radius than others [21], K^+ ions can be an ideal candidate to provide pillar effect between the interplanar spacing of vanadium oxides in order to make material's structure become more stable. Besides, since K^+ ions own longer atomic radius than Zn^{2+}, they can supply larger interplanar spaces between layered crystal structures which can be helpful for repeated Zn^{2+} intercalation/deintercalation [22]. Sambandam et al. [23] was the first scientist who utilized $K_2V_6O_{16}{\cdot}2.7H_2O$ as the cathode for aqueous ZIBs. Nonetheless, K^+ wasn't put into V_2O_5 crystal structure but introduced into V_2O_5's layered structure in order to enlarge the interplanar spacing of V_2O_5, so it didn't really turn into a new phase.

$K_2V_{12}O_{30\text{-}y}{\cdot}nH_2O$ (KVOH) was synthesized by introducing K^+ into the crystal structure of VOH and demonstrated much enhanced electrochemical properties [24]. Similarly when Ni^{2+} was incorporated to VOH, NiVOH as the cathode for aqueous ZIBs possesses a much improved storage property [19].

The introduction of Ni^{2+} to Mn_2O_3 cathode has shown to improve the electronic conductivity, as reported by Zhang et al. [25]. Incorporating transition metal cations such as Ni^{2+} into the cathode material KVOH is expected to get higher value of storage capacity and faster transport kinetics. The present work demonstrated the enhancement of storage capacity and faster transport kinetics after doping transition metals cations such as Ni^{2+} into KVOH, suggesting complex composition may offer some benefits to the electrochemical process.

2. Experimental

2.1. Material synthesis

For synthesizing KNiVOH, 0.364 mg V_2O_5 was added to 50 mL deionized water. And then, 2 mL of H_2O_2 was dripped into the solution as the purpose of activator. 0.086 mg K_2SO_4 and 0.044 mg $NiSO_4$ were added to 30 mL deionized water. Next, these two solutions were mixed together under magnetic agitating for 30 min. After that, the solution was poured into 100 mL Teflon lined stainless steel autoclave and heated up to 120 °C for 6 h. Ultimately, the acquired precipitate was separately washed by deionized water as well as ethanol for three times in succession and then dried in the vacuum oven at 60 °C for 10 h to remove solvent and obtain green powder, named as KNiVOH. In addition, KVOH was synthesized by the same process as Tian et al. [24], and NiVOH was synthesized by the same process as Liu et al. [19]. Furthermore, VOH was prepared in the same conditions as KNiVOH, just without adding K_2SO_4 and $NiSO_4$, and was dried by freeze dryer.

2.2. Characterization

The Bruker D8 Discover was utilized to explore the X-ray diffraction

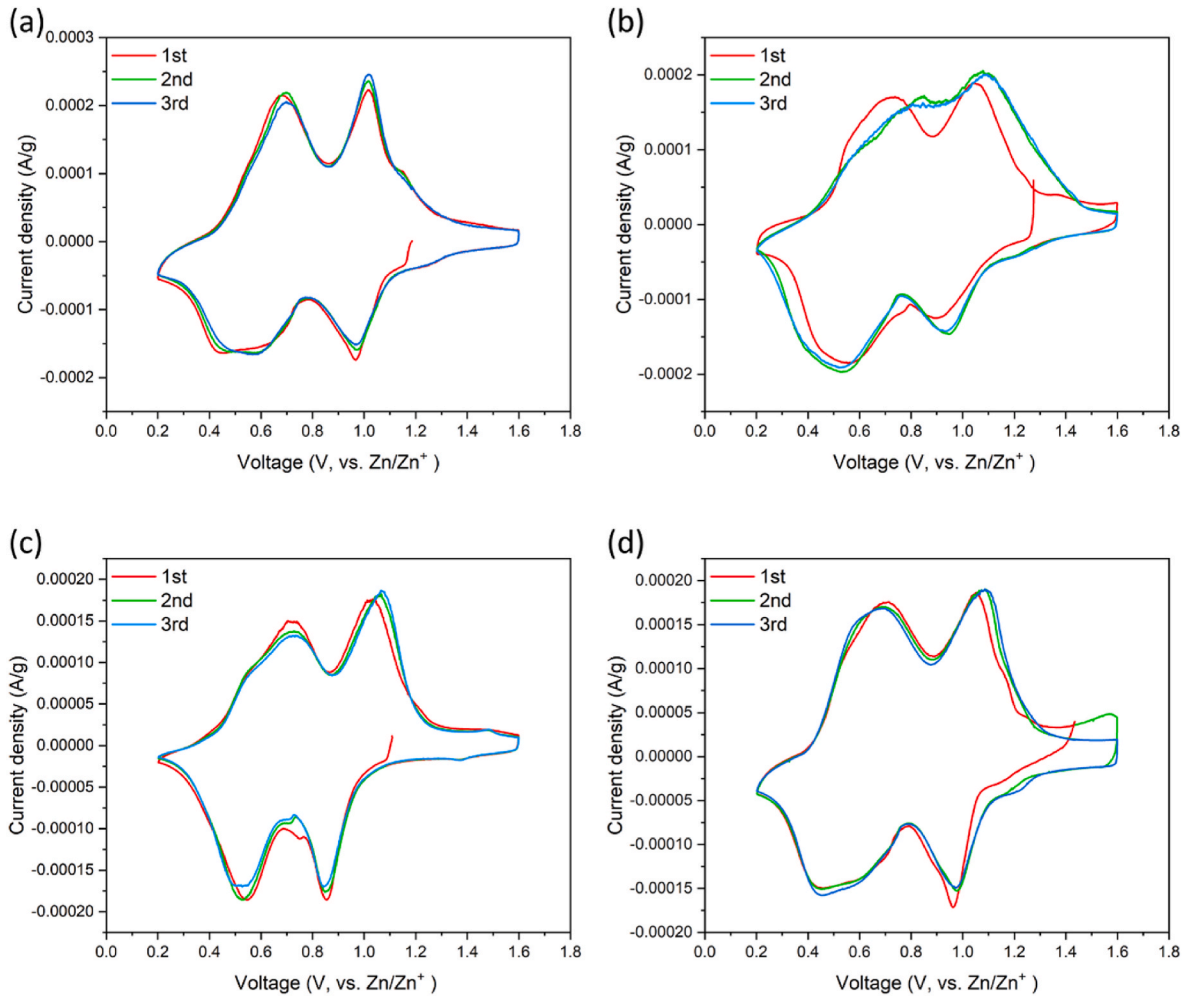

Fig. 4. Initial three CV curves of (a) KNiVOH, (b) KVOH, (c) NiVOH, (d) VOH collected at a scan rate of 0.1 mV s^{-1}.

patterns in order to determine the crystal structures of cathode material samples. The FEI Sirion XL30 SEM, a field-emission scanning electron microscope with an energy-dispersive X-ray spectrometer, was used to obtain information about morphologies and elemental contents of cathode material samples. The Tecnai G2 F20 SuperTwin, a transmission electron microscopy, was also used to acquire the information about morphologies of cathode material samples. The Optima 2000 DV was also used to test elemental contents of cathode material samples by means of inductively coupled plasma (ICP).

2.3. Electrochemical measurements

CR2032 coin cells were utilized to test each cathode materials' electrochemical performance. In order to manufacture cathode electrodes, 35 mg active material, 10 mg carbon black powder and 5 mg polyvinylidene fluoride with concentration of 20 mg/mL were added together by utilizing the mass ratio of 7:2:1 to synthesize and then became the slurry. Next, the slurry was dripped on Titanium foils and dried in auto coater at 60 °C for 1 h. Then, took out the dried cathode electrodes from auto coater and kept on heating them by using vacuum oven at 80 °C for 12 h in order to eliminate remaining solvent.

The ZIB's anode and separator were made of Zn foil and glass fiber filter respectively. The aqueous electrolyte of ZIBs was chosen 3 M Zn $(CF_3SO_3)_2$. The range of voltage value of the test of cyclic voltammetry (CV) and the measurement of electrochemical impedance spectroscopy (EIS) are 0.2–1.6 V and 10^5 to 0.01 Hz respectively. Electrochemical workstation equipped with an electrochemical impedance spectroscope was utilized to carry out the test of CV and the measurement of EIS. The following equation (1) was utilized to acquire the cathode material sample's ion diffusion coefficient value through EIS plots' low frequency section:

$$D_{Zn^{2+}}^{EIS} = \frac{R^2T^2}{2A^2n^4F^4C^2\sigma_w^2} \quad (1)$$

In this equation, the coefficients: A, C, F, R, T, n, and σ_w are separately equal to anode area, ion concentration, Faraday constant, gas constant, absolute temperature, number of electrons transferred as well as Warburg factor. Among these coefficients, Warburg factor σ_w can be calculated from slope value of the line of the best fit for Z′ vs. $\omega^{-1/2}$. The galvanostatic charging/discharging test was implemented by using the Neware tester (CT-4008). The following equation (2) was utilized to calculate the energy density E and equation (3) was utilized to calculate the power density P:

$$E = \int_0^{\Delta t} IV(t)dt \quad (2)$$

$$P = E/t \quad (3)$$

Coefficient I represents current density at various voltage V and t represents the discharge time.

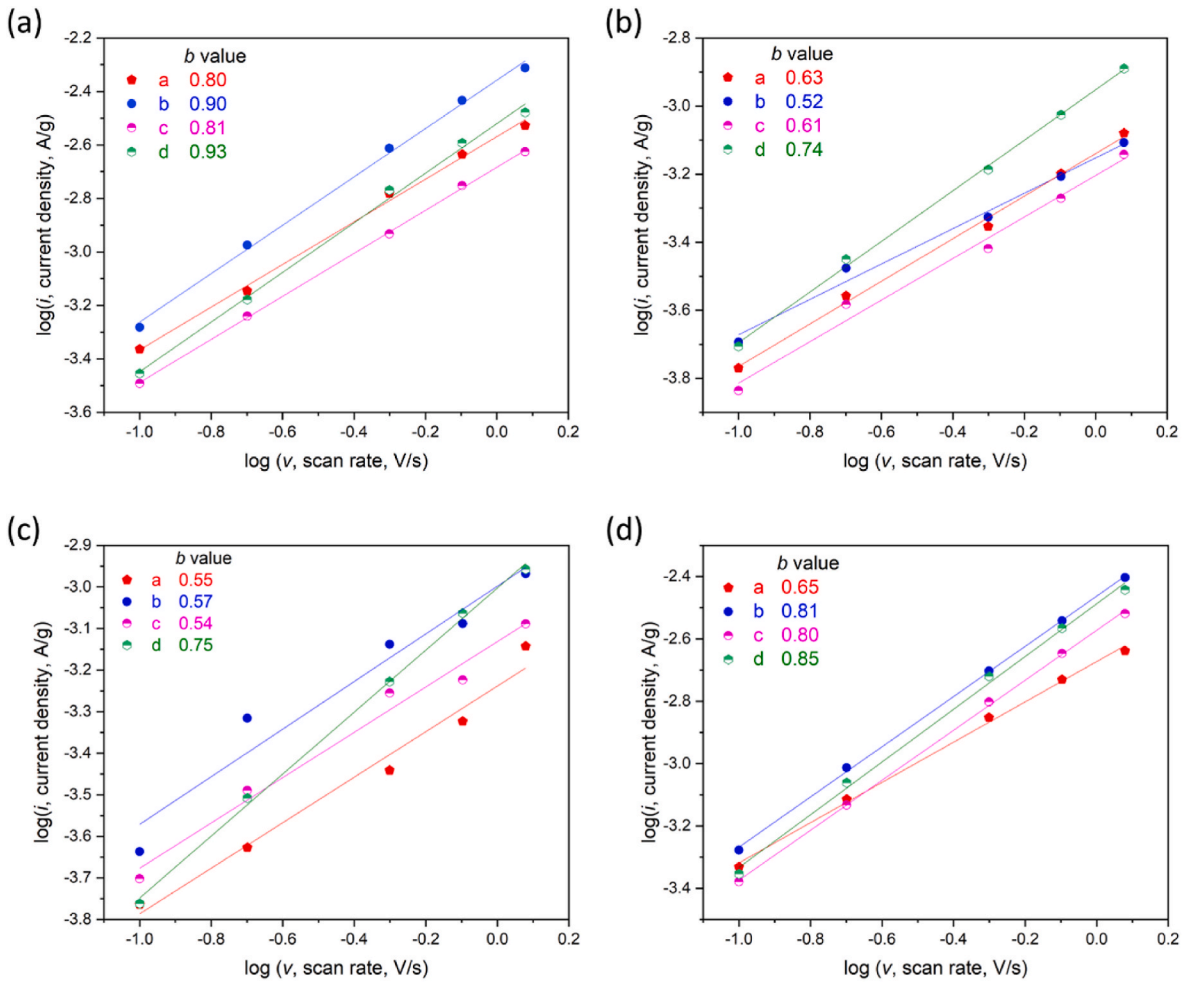

Fig. 5. Plots of four peaks' log i (current density) versus log v (scan rate) in the CV curves of (a) KNiVOH, (b) KVOH, (c) NiVOH and (d) VOH.

3. Results and discussion

The XRD patterns comparison of KNiVOH, KVOH, NiVOH and VOH are shown in Fig. 1a. Since the (001) peak position in VOH's XRD pattern is at 7.4°, the interlayer distance of VOH can be calculated as 11.6 Å by using Bragg equation. Compared to VOH, KNiVOH owns contracted interlayer distance of 11 Å, which is higher than KVOH of 10.8 Å, and it is also similar to the interlayer distance value of 9.9 Å tested by Tian et al. [24] but lower than NiVOH of 11.7 Å. It was proposed that the strong intercalation of potassium ion with oxygen anions in bilayers results in interplanar spacing reduction, which can make KVOH have smaller interlayer spacing than VOH [26]. NiVOH is proposed to be constructed by V_2O_5 bilayers with pre-intercalated Ni^{2+} cations forming NiO_7 polyhedrons [26]. The HR-TEM image shown in Fig. 1b exhibits lattice fringes of KNiVOH with interlayer distance of 0.3 nm, which can match with the (003) plane. The following SEM images of KNiVOH illustrate microspheres with the diameters of 75–80 μm (Fig. 2a), and the microspheres consist of numerous nanorods (Fig. 2b). TEM image confirms the aggregated nanorods (Fig. 2c) with porous structure (Fig. 2d). EDS analysis revealed KNiVOH has an atomic ratio of K:Ni:V equal to1:0.25:10 (in Table S2-1, S2-2), suggesting a formula of $K_4NiV_{40}O_xH_y$, which shows noticeable deviation from starting composition $K_{4.8}Ni_{1.6}V_{40}O_xH_y$, implying some K^+ and Ni^{2+} were not incorporated into V_2O_5 layers. The distribution of each element in the material is presented in the KNiVOH's SEM-EDS pictures (Fig. S1).

Fig. S1 shows the presence of K^+ and Ni^{2+} in the interlayer. XPS spectra shown in Fig. S2a point out the elemental composition of KNiVOH, including V, K, Ni, O, C. A weaker signal of Ni 2p in Fig. S2b suggests the as-synthesized KNiVOH contains trace Ni^{2+}. In K 2p XPS spectra of KVOH and KNiVOH (Fig. S3) also indicate the presence of K^+. Fig. S3 displays a negative shift of K 2p spectrum, caused by the decreased valence in KNiVOH, which is attributed to the incorporation of Ni^{2+} in KNiVOH [27].

The first three cycles CV curves of KNiVOH were gained at 0.1 mV s^{-1} from 0.2 to 1.6 V. The three figures: KNiVOH and KVOH (Fig. 3a), KNiVOH and NiVOH (Fig. 3b), KNiVOH and VOH (Fig. 3c) show the comparison of the third cycle CV curves at 0.1 mV s^{-1}. In these three figures, all curves possess two pairs of redox peaks between 0.6 V and 1.0 V, separately coinciding with V^{4+}/V^{3+} and V^{5+}/V^{4+}. Among these three figures, KVOH's two pairs of redox peaks exhibits the largest voltage gaps. Besides, KNiVOH has higher peak currents than KVOH, NiVOH, and VOH except for V^{4+}/V^{3+} reduction peaks of KVOH and VOH (summarized in Table 1). Compared with KVOH, NiVOH, and VOH, KNiVOH's center positions of V^{4+}/V^{3+} and V^{5+}/V^{4+} separately move from 0.71 to 0.56 V and 1.02 to 0.96 V. The first CV curve of KNiVOH and KVOH (Fig. 3d), KNiVOH and NiVOH (Fig. 3e), KNiVOH and VOH (Fig. 3f) are incomplete since the test was set up to start from the natural open voltage.

In order to have better comparison, fully charged voltage (1.6 V) can be a sign to represent the end of each cycle. There are some small peaks appeared around the position of 1.2 V in KNiVOH, KVOH, NiVOH and VOH, which disappear in the following cycles. It is reasonable assumed that these small peaks are generated due to irreversible side reactions [19,28].

The gap between V^{5+}/V^{4+} redox pairs of KNiVOH is smaller than other three materials in the first cycle (summarized in Table S3). As for

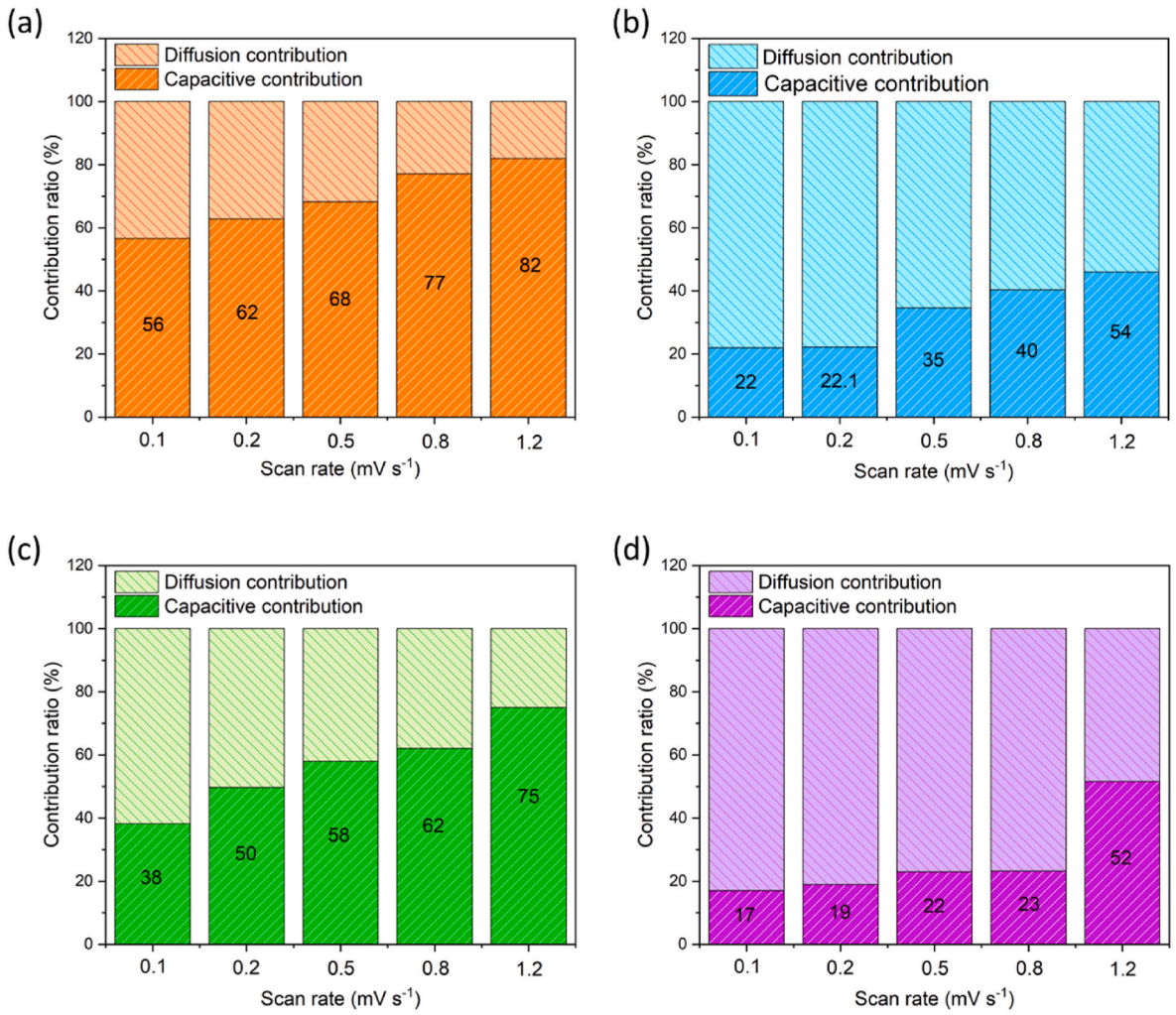

Fig. 6. The capacity contribution at five different scan rates of (a) KNiVOH, (b) KVOH, (c) NiVOH and (d) VOH.

the NiVOH and VOH, the gap in their third cycle CV curves decreases compared to the first cycle CV curves. However, as for the KVOH, the gap in its third cycle CV curves is larger than the first cycle CV curves, and it can be hypothesized that compared with KNiVOH, NiVOH and VOH, KVOH displays the most side reactions in its first cycle.

The similar first three cycles of KNiVOH (Fig. 4a) and NiVOH (Fig. 4c) indicate a similarly reversible redox process. What's more, the first discharge peak around 1V of KNiVOH and NiVOH shift to a higher value of voltage in the following cycles, and it is reasonable assumed that after the insertion of Zn ion, the local environment becomes different. Nevertheless, the first three cycles of KVOH (Fig. 4b) and VOH (Fig. 4d) have diverging peaks, and the second discharge peak which is located near 0.4V moves to lower voltage section in the following cycles.

The equation below contains the coefficients: i, v separately correspond to the peak current and scan rate, which are utilized to calculate the presiding factor controlliong the process of electrochemistry [29]:

$$i = av^b \tag{4}$$

The parameters: a, b are adjustable. As for the parameter b, if its value equals to 1, it means that the process is surface-controlled. Besides, when the value of parameter b is 0.5, the process is diffusion-controlled [30]. The range of b value is from 0.5 to 1, and the redox peaks of KNiVOH, KVOH, NiVOH and VOH conform with different b values. Therefore, it is reasonable assumed that the process is hybrid surface-diffusion controlled.

As for KNiVOH, in Fig. 5a, the b values correspond to its V^{5+}/V^{4+} oxidation peaks and reduction peaks are separately 0.9 and 0.81. Since these values are higher than the values shown in KVOH (Fig. 5b), NiVOH (Fig. 5c) and VOH (Fig. 5d), it can be hypothesized that KNiVOH owns better ion diffusion rate and its reaction is mainly surface-controlled process. Besides, the b values correspond to KNiVOH's V^{4+}/V^{3+} peaks are separately 0.8 and 0.93, which are higher than the b values of KVOH, NiVOH and VOH, and it is reasonable assumed that during charge/discharge cycles, its process is surface-controlled. The current can be equal to capacitive (k_1v) part and diffusion-controlled ($k_2v^{1/2}$) part as shown in the equation below when the voltage is fixed at a scan rate (v):

$$i = k_1v + k_2 \tag{5}$$

In this equation, the coefficients of k_1 and k_2 can be figured out by using Equation (6) in the following:

$$i/v^{1/2} = k_1v^{1/2} + k_2 \tag{6}$$

As for the KNiVOH, 56% and 82% of the capacity are attributed to capacitive contribution at the scan rate of 0.1 mV s^{-1} and 1.2 mV s^{-1} respectively in Fig. 6a. What's more, KNiVOH also shows higher capacitive contribution than KVOH (Fig. 6b), NiVOH (Fig. 6c) and VOH (Fig. 6d), at all scan rates, and this characteristic is advantageous to attain quicker ion diffusion at high scan rates or high current densities.

The Nyquist plots of EIS data of KNiVOH and VOH shown in Fig. 7a display a semicircle part and a linear part in high and low frequency parts respectively. As for the semicircular part before cycling, KNiVOH's charge transfer resistance (R_{ct}) is 146.3 Ω, which is lower than VOH's

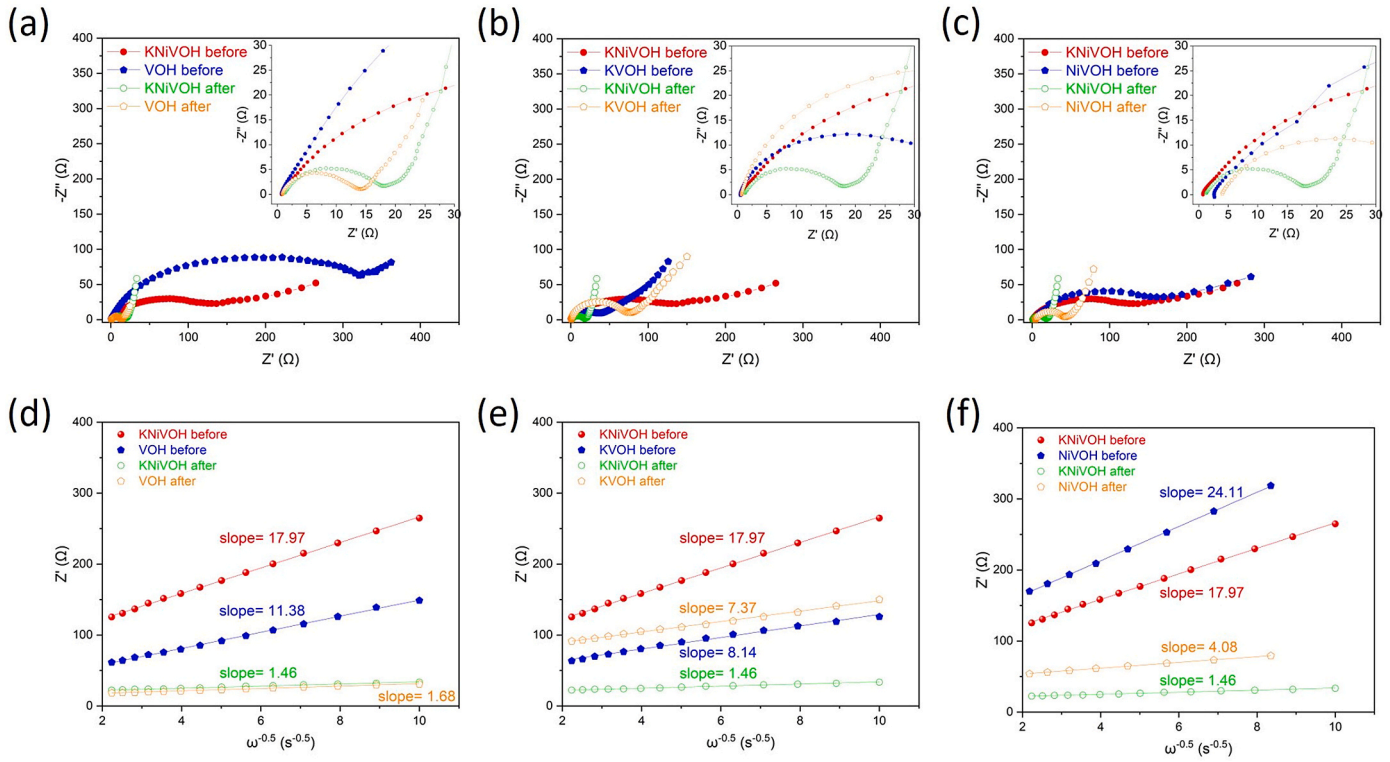

Fig. 7. (a) KNiVOH and VOH, (b) KNiVOH and KVOH, (c) KNiVOH and NiVOH exhibit the Nyquist plots representing both samples' negative imaginary impedance versus the real part of the impedance before and after CV tests. (d) KNiVOH and VOH, (e) KNiVOH and KVOH, (f) KNiVOH and NiVOH exhibit the relationship between low frequencies and the real part of impedance.

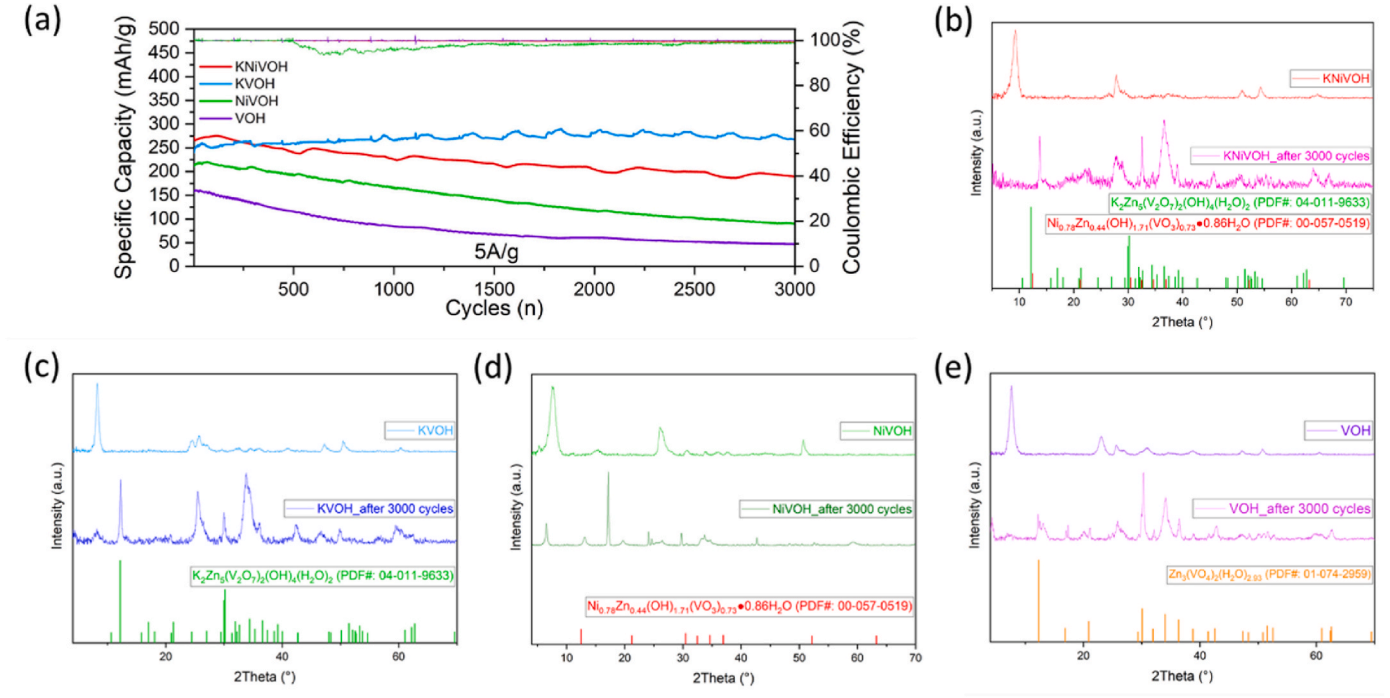

Fig. 8. (a) Cycling stability of KNiVOH, KVOH, NiVOH and VOH at 5 A g^{-1}. XRD patterns of (b) KNiVOH, (c) KVOH, (d) NiVOH and (e)VOH before and after 3000 cycles at 5 A g^{-1}.

value of 393.4 Ω, but higher than pristine KVOH with 42.8 Ω (Fig. 7b) and NiVOH (Fig. 7c) with 131.97 Ω. KNiVOH's R_{ct} value gradually decreases to 17.36 Ω after 15 times CV cycles, which is similar to VOH with 13.72 Ω (Fig. 7a) but lower than KVOH with 77.49 Ω (Fig. 7b) and NiVOH (Fig. 7c) with 24.01 Ω. Ion diffusion coefficients (D_{Zn}^{2+}) can be evaluated by the slope values of linear part of curves made from low frequencies versus the real part of impedance in Fig. 7d–7f [31]. KNiVOH in the pristine state represents D_{Zn}^{2+} value of 1.24×10^{-12} cm^2 s^{-1}

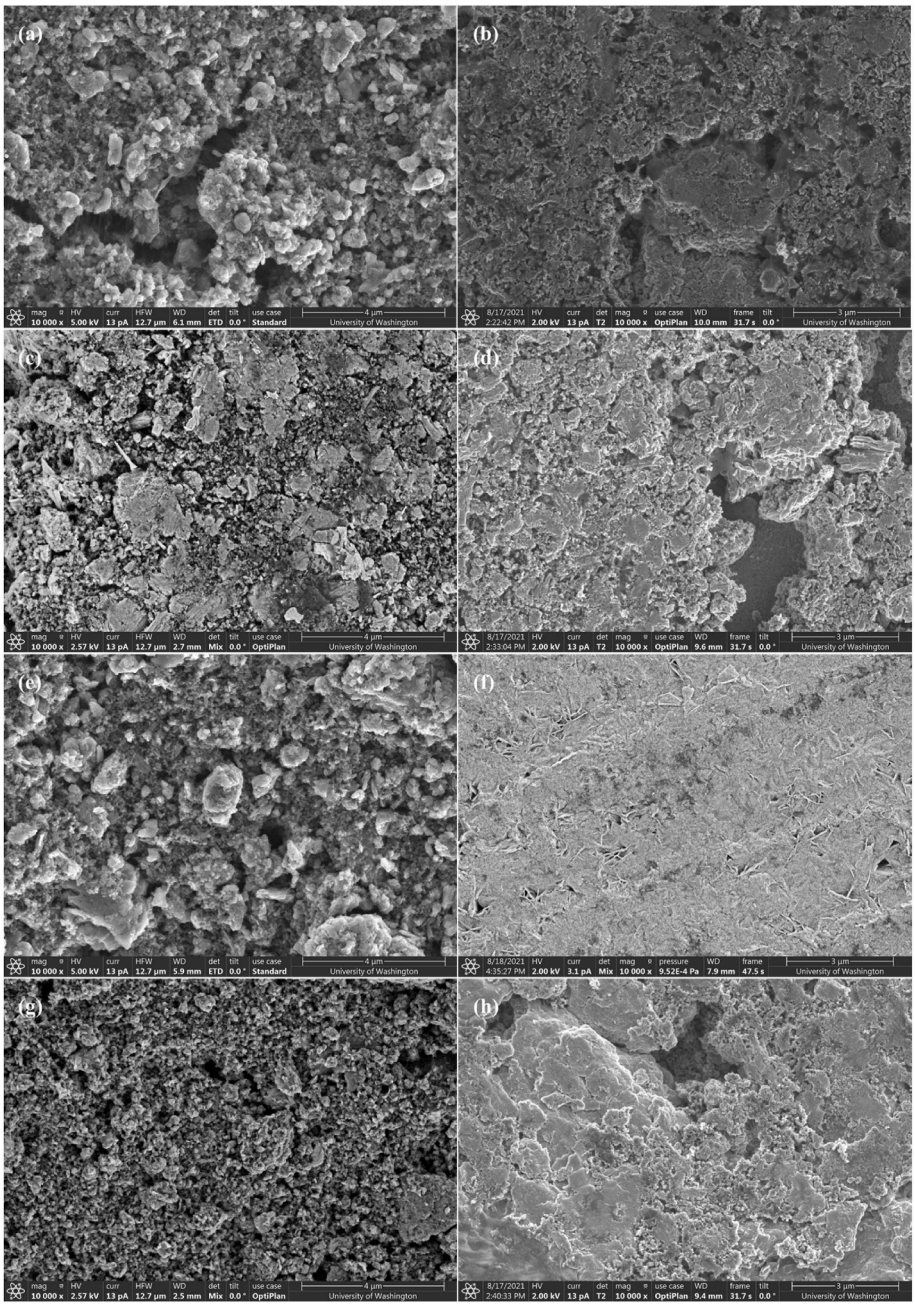

Fig. 9. SEM images of (a) KNiVOH, (c) KVOH, (e) NiVOH and (g) VOH before and (b) KNiVOH, (d) KVOH, (f) NiVOH and (h) VOH after 3000 cycles at 5 A g^{-1}.

which is lower than VOH (3.08×10^{-12} cm^2 s^{-1}) in Fig. 7d as well as KVOH (6.02×10^{-12} cm^2 s^{-1}) in Fig. 7e but higher than NiVOH (6.86×10^{-13} cm^2 s^{-1}) in Fig. 7f respectively. After 15 times of CV cycles, along with reduced R_{ct}, the diffusion coefficient of KNiVOH is raised to 1.87×10^{-10} cm^2 s^{-1}, which is separately higher than VOH (1.41×10^{-10} cm^2 s^{-1}) in Fig. 7d, KVOH (7.34×10^{-12} cm^2 s^{-1}) in Fig. 7e and NiVOH (2.40×10^{-11} cm^2 s^{-1}) in Fig. 7f. This phenomenon can be hypothesized that due to the trapped Zn^{2+}, the improvement in electro-activation process and electrodes' wettability can be accomplished. Besides, the reason for raising capacities value at the very beginning of the cycling process can also be ascribed to the trapped Zn^{2+}. Fig. 8a compares the cycling stability and coloumbic efficiencies at 5A g^{-1}. KNiVOH has an original capacity of 266 mAh g^{-1}, continuously increasing to 275 mAh g^{-1} at 120 cycle. First of all, the fully infiltrated of electrolyte result in the improvement in utilizing active material [32]. Also, the [VO_n] interlayers can be connected by the trapped Zn ion in order to supply more paythways for charge transfer and result in lower value of resistance, and this phenomenon can be certified by the larger value of initial R_{ct} compared with the value of R_{ct} after the CV cycles. Secondly, as above mentioned, KNiVOH's ion diffusion coefficient is raised by two orders of magnitude after the activation, which is more remarkable than the growth of KVOH, NiVOH and VOH. This difference can be reasonably hypothesized that the inhibition of potassium dissolution through the incorporation of Ni^{2+} to intrinsically stabilize K–O bond. In addition, the Ni^{2+} doped into KVOH lattice will improve the reaction kinetics as well as electrochemical performance of the KNiVOH through electronic rearrangement and facilitation of the H^+ ions or Zn^{2+} ions [25]. KNiVOH displays a high specific capacity value of 275 mAh g^{-1} (5 A g^{-1}) during the 200 cycles in cycling performance, which is more than KVOH (266 mAh g^{-1}). Although KNiVOH initially outperformed KVOH, its specific capacity decays fast and became lower than that of KVOH. While the exact mechanisms are not known, Zhang et al. [25] reported

that excessive Ni^{2+} incorporation has a disadvantageous effect on the performance of cathode material because of the formation of NiO and the reduction of active potassium species such as $K_{4.8}Ni_{1.6}V_{40}O_xH_y$.

Fig. S4 compares the rate capability between KNiVOH and VOH, KNiVOH and KVOH, KNiVOH and NiVOH at different current densities. GCD curves of KNiVOH in Fig. S5 reveals a discharge capacity of 414 mAh g^{-1} at 50 mA/g, and Table S4 compares the specific capacitance at a current density of 50 mA/g with a few cathode materials in aqueous zinc-ion batteries. The ex-situ XRD patterns of KNiVOH (Fig. 8b), KVOH (Fig. 8c), NiVOH (Fig. 8d) and VOH (Fig. 8e) exhibit the difference between the virgin phase and the phase that has gone through 3000 cycles charge/discharge process. Some peaks come out after 3000 cycles, which cannot correspond to the XRD patterns of VOH: $V_2O_5{\cdot}1.6H_2O$ (JSPDS, No. 40–1296); it is reasonable assumed that the reactions between air and the drying electrolyte during battery dissemble may produce some by-products. For KNiVOH and KVOH, we can see $K_2Zn_5(V_2O_7)_2(OH)_4{\cdot}(H_2O)_2$ (PDF#: 04-011-9633) appear. In addition, $Ni_{0.78}Zn_{0.44}(OH)_{1.71}(VO_3)_{0.73}{\cdot}0.86H_2O$ (PDF#: 00-057-0519) pattern can match with NiVOH, and VOH has high compatibility with the pattern of $Zn_3(VO_4)_2(H_2O)_{2.93}$ (PDF#: 01-074-2959). What's more, these results can be reasonably assumed that in the aqueous electrolyte, Zn^{2+} commonly could react with H_2O molecules to form large $[Zn(H_2O)_6]^{2+}$ [22]. The Zn^{2+} in H_2O could abate the O–H bond, and the fractured O–H bond would generate OH^- and react with VO in the layered structures to produce $Zn_3V_2O_7(OH)_2{\cdot}2H_2O$. Meanwhile, it is reasonable assumed that the generated H^+ would be inserted into the microstructure of cathode materials but not exist in the electrolyte [33]. Besides, in the process of 3000 cycles charging-discharging, compare with Fig. 1a, we can observe the broadening and the decrease in the intensity of their (001) peaks, which can be hypothesized to the reduction of particle size [32].

The (001) peaks of KNiVOH, KVOH and VOH shift to higher angle section, which means that the decrease in the interplanar spacing of these three materials during the intercalation of Zn^{2+}. What's more, it can also be hypothesized that the reason for shrinkage in the interlayer spacing is caused by the forceful electrostatic reaction between Zn^{2+} and negative single-connected oxygen.

However, only the (001) peak of NiVOH shifts to lower angle section, and the intensity value of its (001) peak doesn't weaken, which means that its interlayer spacing become larger, and it is reasonable assumed that this phenomenon is owing to the Zn^{2+} getting stuck in the ion paths of (001) plane, so the interlayer spacing become larger than before. However, since Zn^{2+} get stuck in the ion paths and cannot intercalate/deintercalate as conveniently as before, its performance of conductivity become poorer and makes it has lower value of specific capacity than KNiVOH and KVOH, which can match with the result in Fig. 8a.

Fig. 9a−9h are SEM images of KNiVOH, KVOH, NiVOH and VOH before and after 3000 charge/discharge cycles at 5 A g^{-1}. We can see NiVOH and VOH in Fig. 9f & h seperatively show severe aggregation compared to KNiVOH and KVOH (Fig. 9b and d), which induces irreversibility and undesirable cycling performance. Moreover, this phenomenon can match with the result of cycling stability in Fig. 8a, since after 3000 cycles, KNiVOH can still remain its stability with 43.2% decay in capacity value, and the capacity value of KVOH even increases by 9.5% after 3000 cycles. Nevertheless, NiVOH and VOH both keep low stability with 57.4% and 70.2% fading after 3000 cycles separately. Hence, it is a practical strategy to combine potassium with other transition metals to synthesize new cathode materials for ZIBs in the future.

4. Conclusions

KNiVOH as ZIBs' cathode material demonstrated high capacity and good cycle performance. Incorporating of Ni^{2+} is believed to facilitate the electronic conductivity, and the zinc ion intercalation kinetics in KNiVOH. The voltage gap of the redox pair V^{5+}/V^{4+} in KNiVOH is the smallest compared to VOH, KVOH and NiVOH; KNiVOH has the smallest polarization. KNiVOH possesses the highest capacitive contribution than other three materials at five different scan rates, due to its fast transport property. KNiVOH delivers a capacity (275 mAh g^{-1}) at 5A g^{-1} than KVOH (266 mAh g^{-1}).

Funding

This work was supported by the National Science Foundation Grant number CBET-1803256.

CRediT authorship contribution statement

Sean Li: Methodology, Investigation, Formal analysis, Writing – original draft. **Xiaoxiao Jia:** Visualization, Project administration. **Junchao Liu:** Writing – review & editing. **Ziyan Liu:** Validation, Conceptualization. **Guozhong Cao:** Supervision, Funding acquisition.

Declaration of competing interest

The authors declare the following financial interests/personal relationships which may be considered as potential competing interests: Guozhong Cao reports financial support was provided by National Science Foundation (CBET-1803256).

Acknowledgements

We appreciate greatly National Science Foundation (CBET-1803256) sponsoring us this work.

Appendix A. Supplementary data

Supplementary data to this article can be found online at https://doi.org/10.1016/j.matchemphys.2022.126358.

References

[1] M.S. Whittingham, Electrical energy storage and intercalation chemistry, Science 192 (1976) 1126–1127.
[2] Y. Ding, C. Zhang, L. Zhang, Y. Zhou, G. Yu, Molecular engineering of organic electroactive materials for redox flow batteries, Chem. Soc. Rev. 47 (2018) 69–103.
[3] B. Tang, L. Shan, S. Liang, J. Zhou, Issues and opportunities facing aqueous zinc-ion batteries, Energy Environ. Sci. 12 (2019) 3288–3304.
[4] Z. Xing, S. Wang, A. Yu, Z. Chen, Aqueous intercalation-type electrode materials for grid-level energy storage: beyond the limits of lithium and sodium, Nano Energy 50 (2018) 229–244.
[5] C. Xia, J. Guo, Y.J. Lei, H.F. Liang, C. Zhao, H.N. Alshareef, Rechargeable aqueous zinc-ion battery based on porous framework zinc pyrovanadate intercalation cathode, Adv. Mater. 30 (2018), 1705580.
[6] J. Liu, C. Xu, Z. Chen, S. Ni, Z.X. Shen, Progress in aqueous rechargeable batteries, Green Energy Environ. 3 (2018) 20–41.
[7] L. Jiang, Y. Lu, C. Zhao, L. Liu, J. Zhang, Q. Zhang, X. Shen, J. Zhao, X. Yu, H. Li, X. Huang, L. Chen, Y.-S. Hu, Building aqueous K-ion batteries for energy storage, Nat. Energy 4 (2019) 495–503.
[8] D. Yuan, J. Zhao, W. Manalastas, S. Kumar, M. Srinivasan, Emerging rechargeable aqueous aluminum ion battery: status, challenges, and outlooks, Nano Mater. Sci. 2 (2019) 248–263.
[9] M. Song, H. Tan, D. Chao, H.J. Fan, Recent advances in Zn-ion batteries, Adv. Funct. Mater. 28 (2018), 1802564.
[10] X. Jia, C. Liu, Z. Neale, J. Yang, G. Cao, Active materials for aqueous zinc ion batteries: synthesis, crystal structure, morphology, and electrochemistry, Chem. Rev. 120 (2020) 7795–7866.
[11] T. Xiong, Z.G. Yu, H. Wu, Y. Du, Q. Xie, J. Chen, Y. Zhang, S.J. Pennycook, W. Siang, V. Lee, J. Xue, Defect engineering of oxygen-deficient manganese oxide to achieve high-performing aqueous zinc ion battery, Adv. Energy Mater. 9 (2019), 1803815.
[12] J. Zheng, C. Liu, M. Tian, X. Jia, E.P. Jahrman, G.T. Seidler, S. Zhang, Y. Liu, Y. Zhang, C. Meng, G. Cao, Fast and reversible zinc ion intercalation in Al-ion modified hydrated vanadate, Nano Energy 70 (2020), 104519.
[13] Y. Zhang, H. Jiang, L. Xu, Z. Gao, C. Meng, Ammonium vanadium oxide $[(NH_4)_2V_4O_9]$ sheets for high capacity electrodes in aqueous zinc ion batteries, ACS Appl. Energy Mater. 2 (2019) 7861–7869.
[14] D. Chao, C.(R. Zhu, M. Song, P. Liang, X. Zhang, N.H. Tiep, H. Zhang, H.J. Fan, High-rate and stable quasi–solid–state zinc-ion battery with novel 2D layered zinc orthovanadate array, Adv. Mater. 30 (2018), 1803181.

[15] L. Shan, Y. Yang, W. Zhang, H. Chen, G. Fang, J. Zhou, S. Liang, Observation of combination displacement/intercalation reaction in aqueous zinc-ion battery, Energy Storage Mater. 18 (2019) 10–14.
[16] T. Wu, K. Zhu, C. Qin, K. Huang, Unraveling the role of structural water in bilayer V_2O_5 during Zn^{2+}-intercalation: insights from DFT calculations, J. Mater. Chem. 7 (2019) 5612–5620.
[17] S. Guo, G. Fang, S. Liang, M. Chen, X. Wu, J. Zhou, Structural perspective on revealing energy storage behaviors of silver vanadate cathodes in aqueous zinc-ion batteries, Acta Mater. 180 (2019) 51–59.
[18] Y. Yang, Y. Tang, S. Liang, Z. Wu, G. Fang, X. Cao, C. Wang, T. Lin, A. Pan, J. Zhou, Transition metal ion-preintercalated V_2O_5 as high-performance aqueous zinc-ion battery cathode with broad temperature adaptability, Nano Energy 61 (2019) 617–625.
[19] C. Liu, Z. Neale, J. Zheng, X. Jia, J. Huang, M. Yan, M. Tian, M. Wang, J. Yang, G. Cao, Expanded hydrated vanadate for high-performance aqueous zinc–ion batteries, Energy Environ. Sci. 12 (2019) 2273–2285.
[20] S. Islam, H. Alfaruqi, B. Sambandam, A new rechargeable battery based on a zinc anode and a NaV_6O_{15} nanorod cathode, Chem. Commun. 55 (2019) 3793–3796.
[21] J. Zhong, D. Chen, X. Chen, K. Wang, X. Li, Y. Zhu, Z. Ji, Efficient rare-earth free red-emitting Ca_2YSbO_6:Mn^{4+}, M (M = Li^+, Na^+, K^+, Mg^{2+}) phosphors for white light-emitting diodes, Dalton Trans. 47 (2018) 6528–6537.
[22] B. Tang, G. Fang, J. Zhou, L. Wang, Y. Lei, C. Wang, T. Lin, Y. Tang, S. Liang, Potassium vanadates with stable structure and fast ion diffusion channel as cathode for rechargeable aqueous zinc-ion batteries, Nano Energy 51 (2018) 579–587.
[23] B. Sambandam, V. Soundharrajan, S. Kim, M.H. Alfaruqi, J. Jo, S. Kim, V. Mathew, Y.-k. Sun, J. Kim, $K_2V_6O_{16}{\cdot}2.7H_2O$ nanorod cathode: an advanced intercalation system for high energy aqueous rechargeable Zn-ion batteries, J. Mater. Chem. 6 (2018) 15530–15539.
[24] M. Tian, C. Liu, J. Zheng, X. Jia, E.P. Jahrman, G.T. Seidler, D. Long, M. Atif, M. Alsalhi, G. Cao, Structural engineering of hydrated vanadium oxide cathode by K^+ incorporation for high-capacity and long-cycling aqueous zinc ion batteries, Energy Storage Mater. 29 (2020) 9–16.
[25] D. Zhang, J. Cao, X. Zhang, N. Insin, S. Wang, J. Han, Y. Zhao, J. Qin, Y. Huang, Inhibition of manganese dissolution in Mn_2O_3 cathode with controllable Ni^{2+} incorporation for high-performance zinc ion battery, Adv. Funct. Mater. 31 (2021), 2009412.
[26] C. Xia, J. Guo, P. Li, X.X. Zhang, H.N. Alshareef, Highly stable aqueous zinc-ion storage using a layered calcium vanadium oxide bronze cathode, Angew. Chem. Int. Ed. 57 (2018) 3943.
[27] N. Zhang, F. Cheng, Y. Liu, Q. Zhao, K. Lei, C. Chen, X. Liu, J. Chen, Cation-Deficient spinel $ZnMn_2O_4$ cathode in $Zn(CF_3SO_3)^2$ electrolyte for rechargeable aqueous Zn-ion battery, Am. Chem. Soc. 138 (2016), 12894.
[28] C. Xie, Y. Li, Q. Wang, D. Sun, Y. Tang, H. Wang, Issues and solutions toward zinc anode in aqueous zinc-ion batteries: a mini review, Carbon Energy 2 (2020) 540–560.
[29] P. Hu, T. Zhu, X. Wang, X. Wei, M. Yan, J. Li, W. Luo, W. Yang, W. Zhang, L. Zhou, Z. Zhou, L. Mai, Highly durable $Na_2V_6O_{16}{\cdot}1.63H_2O$ nanowire cathode for aqueous zinc-ion battery, Nano Lett. 18 (2018) 1758–1763.
[30] H. Jiang, Y. Zhang, L. Xu, Z. Gao, J. Zheng, Q. Wang, C. Meng, J. Wang, Fabrication of $(NH_4)_2V_3O_8$ nanoparticles encapsulated in amorphous carbon for high capacity electrodes in aqueous zinc ion batteries, Chem. Eng. J. 382 (2020), 122844.
[31] C. Yin, C. Pan, X. Liao, Y. Pan, L. Yuan, Coordinately unsaturated manganese-based metal-organic frameworks as a high-performance cathode for aqueous zinc-ion batteries, ACS Appl. Mater. Interfaces 13 (2021) 35837–35847.
[32] M. Du, C. Liu, F. Zhang, W. Dong, X. Zhang, Y. Sang, J. Wang, Y. Guo, H. Liu, S. Wang, Tunable layered $(Na,Mn)V_8O_{20}{\cdot}nH_2O$ cathode material for high-performance aqueous zinc ion batteries, Adv. Sci. 7 (2020), 2000083.
[33] F. Wan, L. Zhang, X. Dai, X. Wang, Z. Niu, J. Chen, Aqueous rechargeable zinc/sodium vanadate batteries with enhanced performance from simultaneous insertion of dual carriers, Nat. Commun. 9 (2018) 1656.